Solid State Electronics 140 (2018) 109–114

Contents lists available at ScienceDirect

Solid State Electronics

journal homepage: www.elsevier.com/locate/sse

Effect of liquid gate bias rising time in pH sensors based on Si nanowire ion sensitive field effect transistors

Jungkyu Jang[a,1], Sungju Choi[a,1], Jungmok Kim[a], Tae Jung Park[b], Byung-Gook Park[c], Dong Myong Kim[a], Sung-Jin Choi[a], Seung Min Lee[a], Dae Hwan Kim[a,*], Hyun-Sun Mo[a,**]

[a] School of Electrical Engineering, Kookmin University, Seoul 02707, Republic of Korea
[b] Department of Chemistry, Chung-Ang University, Seoul 06974, Republic of Korea
[c] Department of Electrical and Computer Engineering, Seoul National University, Seoul 151-742, Republic of Korea

ARTICLE INFO

Keywords:
Liquid gate bias
Rising time
Transient response
ISFET
Si nanowire
Drift/diffusion of mobile ions in analyte

ABSTRACT

In this study, we investigate the effect of rising time (T_R) of liquid gate bias (V_{LG}) on transient responses in pH sensors based on Si nanowire ion-sensitive field-effect transistors (ISFETs). As T_R becomes shorter and pH values decrease, the ISFET current takes a longer time to saturate to the pH-dependent steady-state value. By correlating V_{LG} with the internal gate-to-source voltage of the ISFET, we found that this effect occurs when the drift/diffusion of mobile ions in analytes in response to V_{LG} is delayed. This gives us useful insight on the design of ISFET-based point-of-care circuits and systems, particularly with respect to determining an appropriate rising time for the liquid gate bias.

1. Introduction

An important indicator in industries such as food, pharmaceutical, agriculture, biomedical, and environmental monitoring is pH; for example, variations in pH of human blood are signs of serious, potentially fatal diseases [1]. The solubility, stability, and permeability of a drug through biological membrane also depend on pH [2], and therefore, a precise pH measurement technique using a miniaturized sensor is essential. Furthermore, the solubility of heavy metals such as lead, zinc, and copper in soil is dependent on the pH [3], and therefore, pH measurement is important for managing the environment.

Ion-sensitive field-effect transistors (ISFETs) [4] have attracted considerable attention because of their compact structure, low-cost, and ease of fabrication. Recently, ISFET-based pH sensors have been successfully used in human genome sequencing [5–7]. The resolution of an ISFET-based pH sensor depends on its individual technology and geometry. Therefore, optimum operation of the sensor in complex analog circuits where biasing configuration may change over time needs to be anticipated. The transient response of an ISFET-based pH sensor is governed by two processes: the convection/diffusion of H^+ ions to the sensor surface (diffusion time) and the response of the sensor to the changes in proton concentration on its surface (response time). Diffusion time depends on various factors that define the ion transport time to the sensor, such as flow rate and the size/shape of the fluidic channel. However, the transient response to time-varying liquid gate bias (V_{LG}) has been rarely investigated despite its importance. To optimize the details of operation, particularly the choice of the saturation time of signals in the ISFET-based point-of-care (PoC) circuits, the influence of the rising time of V_{LG} needs to be experimentally characterized. We studied ways to simplify the properties that may affect the way the sensor works. For example, we measured droplets before they entered the microfluidic channel. In this way, we could exclude complicated factors such as convection and diffusion in the analyte.

Conversely, the silicon nanowire (SiNW) ISFET-based biosensors have great potential as essential building blocks for real-time, label-free detection of biomolecules because of their advantages such as direct electrical readouts and high sensitivity and the potential to integrate them with complementary metal–oxide semiconductor (CMOS) circuits [8–11]. Based on the top-down processing in the SiNW/CMOS hybrid circuitry, researchers have already demonstrated electrical optimization sensitivity [12], sensitivity boosting [13], voltage readout [14], noise cancellation [15], and simulation using commercial technology computer aided design (TCAD) [16]. It should therefore be noted that operating the SiNW ISFET in the saturation region is desirable for a robust analog front-end design, although the ISFET sensitivity itself can be better in the sub-threshold rather than the saturation region.

* Corresponding author.
** Corresponding author.
E-mail addresses: drlife@kookmin.ac.kr (D.H. Kim), tyche@kookmin.ac.kr (H.-S. Mo).
[1] Contributed equally to this work.

http://dx.doi.org/10.1016/j.sse.2017.10.027

Available online 12 October 2017

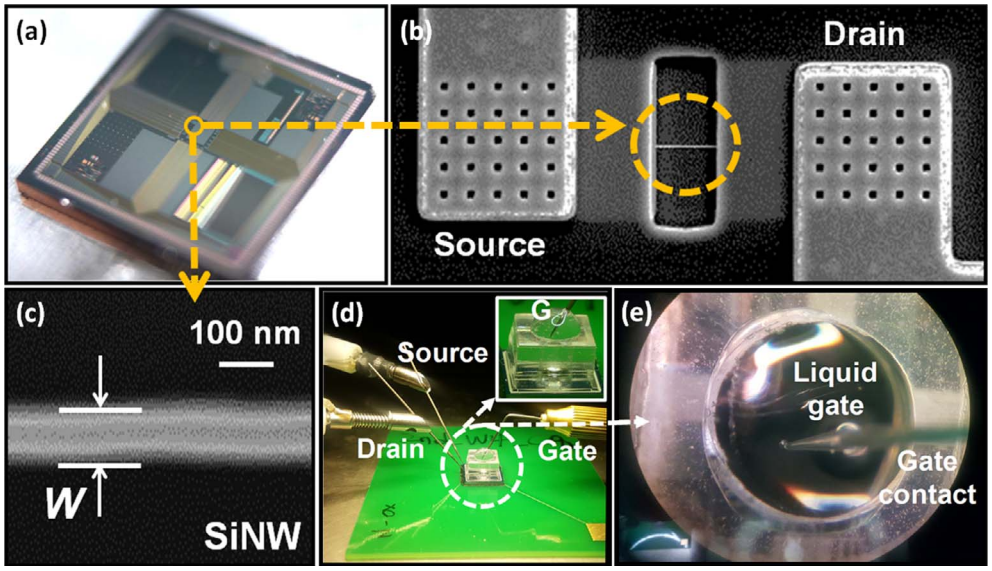

Fig. 1. Photo of the (a) fabricated chip, (b) the SiNW biosensor, (c) the SiNW channel region, and (d) the measurement environment. (e) Top view of the liquid gate region.

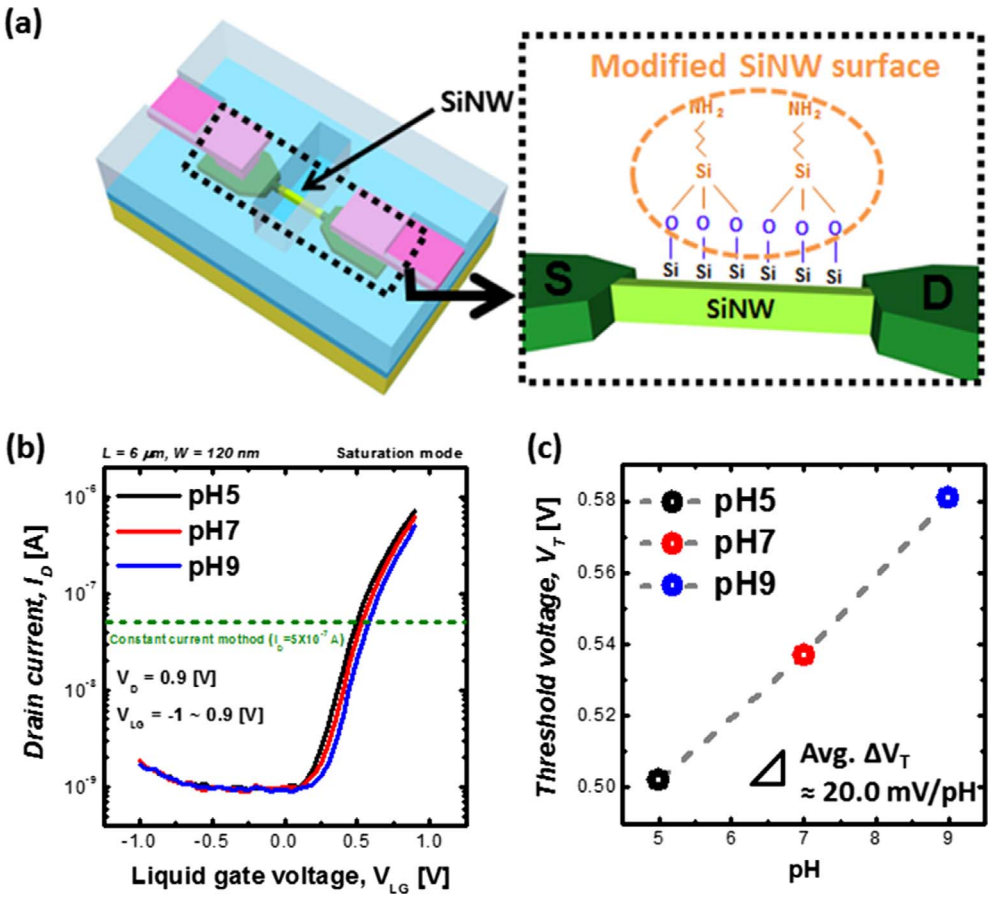

Fig. 2. (a) Bird's-eye view of the surface treated SiNW biosensor. (b) Transfer curve of SiNW FET measured in saturation mode using under the different pH. (c) ΔV_T extracted by constant current method (at I_D = 1 nA) of SiNW FET.

In this work, the influence of the V_{LG} rising time (T_R) on transient current response in the top-down processed SiNW ISFET-based pH sensors operating in the saturation region is investigated. By correlating V_{LG} with the internal gate-to-source voltage of ISFET ($V_{GS,int}$) at the electrolyte/insulator interface, we have gained new physical and chemical insights into the drift/diffusion of mobile ions in an electrolyte analyte.

2. SiNW ISFET: Fabrication and experiments

SiNW ISFET-based pH sensors were fabricated on a boron-doped (4×10^{15} cm^{-3}) 6-inch (1 0 0) silicon-on-insulator wafer. The 100 nm-thick Si layer at the top was separated from the Si substrate by a 375 nm thick buried oxide (BOX). To build the buffer oxide as protection for implantation, a 20 nm thick SiO_2 layer was formed on top of the Si layer by dry oxidation. As a result, the thickness of the top Si layer was reduced to 90 nm. Subsequently, channel implantation was conducted for the p-type region (B^+, energy: 20 keV, dose: 5×10^{13} cm^{-2}) and the n-

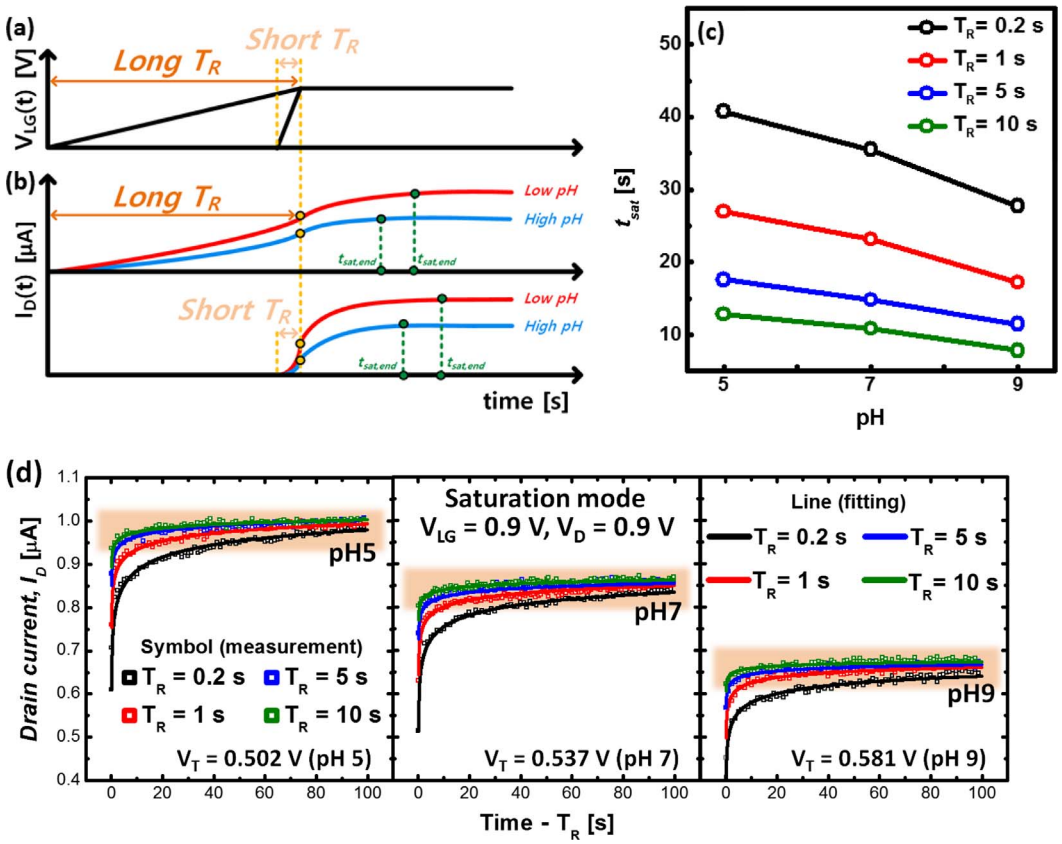

Fig. 3. Schematics of (a) V_{LG}-time and (b) I_D-time under the different pH and T_R. (c) The graph of t_{sat}-pH under the different T_R. (d) The experimental results of I_D-(time-T_R) under different T_Rs (0.2 s, 1 s, 5 s, and 10 s) and the different pH level (0.1 M potassium phosphate buffer, pH 5 - 9).

Table 1
Summarized effects of T_R and pH on t_{sat}.

t_{sat} [s]			
	pH		
T_R	5	7	9
0.2 s	40.78	35.51	27.76
1 s	27.01	23.19	17.25
5 s	17.59	14.86	11.46
10 s	12.88	10.87	7.84

type region (P^+, energy: 40 keV, dose: 3×10^{13} cm^{-2}). After stripping the buffer oxide in a HF solution, the annealing process was conducted at 950 °C for 30 min. Subsequently, the device-active region was patterned on the Si layer via a mix-and-match process of electron-beam (e-beam) lithography combined with conventional photolithography. The 90 nm thick Si layer was anisotropically etched in the HBr/O_2-based inductively coupled plasma chamber by using hydrogen silsesquioxane (HSQ) and photoresist (PR) as the etch mask. A PR mask, which covered only the SiNW channel, was used to dope the source/drain regions of the SiNW with As^+ ion implantation for an n-type source/drain. After PR stripping, the annealing step followed at 1000 °C for 30 min to activate the dopant. The next step was to deposit a 500 nm oxide as an interlayer dielectric using high-density plasma chemical vapor deposition. Subsequently, we applied chemical mechanical planarization. A contact hole was then formed by photolithography and magnetic-enhanced reactive ion etching (MERIE) in a CHF_3/CF_4 plasma. After metallization using Al sputtering, photolithography, and MERIE in BCl_2/Cl_2 plasma, tetraethyl orthosilicate (TEOS) was deposited as a passivating oxide to protect the metal lines. For electrical measurement, the oxide layer on the metal pad region was etched by photolithography and MERIE in CHF_3/CF_4 plasma. Finally, we removed the TEOS passivation oxide using MERIE in CHF_3/CF_4 plasma so that the sensing area on the SiNW channel region became open and connected with the SiNW surface and the biomolecule analyte. The completion of alloy fabrication marked the end of the entire process. A photograph of the fabricated chip is shown in Fig. 1(a). Scanning electron microscope images of the SiNW ISFET biosensor and the SiNW itself are shown in Fig. 1(b) and (c). The measurement environment is shown in Fig. 1(d) and (e); Fig. 1 (e) shows the enlarged liquid gate contacting the reference electrode (RE).

In the pH-sensing experiments, the SiO_2 surface of the SiNWs was modified with 3-aminopropyltriethoxysilane (APTES). A schematic bird's eye view of the surface-modified SiNW is shown in Fig. 2(a). Surface-modified SiNW ISFET was then exposed to 0.1 × potassium phosphate buffer solutions with three different pH values (i.e., pH 5, 7, and 9) by dropping buffer solutions onto a polydimethylsiloxane (PDMS) container as seen in Fig. 1(d). The drain current (I_D) is measured at room temperature at a constant drain/source voltage (V_D/V_S) of 0.9/0 V while V_{LG} was swept from −1 to 1.2 V with 25 mV steps by using a Ag/AgCl reference electrode, as seen in Fig. 1(e). The transfer characteristics of the n-type SiNW ISFET for the three different pH values are shown in Fig. 2(b). The gate leakage current is negligible. As the pH levels increase, the conductance of the n-type SiNW FET decreases, resulting in a positive shift of the threshold voltage (V_T). This can be explained by the protonation/deprotonation of $-NH_2$ and $-SiOH$ groups on the functionalized SiNW surface. At low pH levels, the $-NH_2$ group is protonated to $-NH_3$, resulting in a positive charge. By contrast, at high pH levels, the $-SiOH$ group is deprotonated to $-SiO^-$ and results in a negative charge [17]. The average V_T shift (ΔV_T) is 20 mV per pH [Fig. 2(c)], which is below the Nernst limit as expected. Small ΔV_T is caused by non-ideal interfaces between the gate insulator layer and electrolyte [18]. Although the ΔV_T sensitivity is lower than

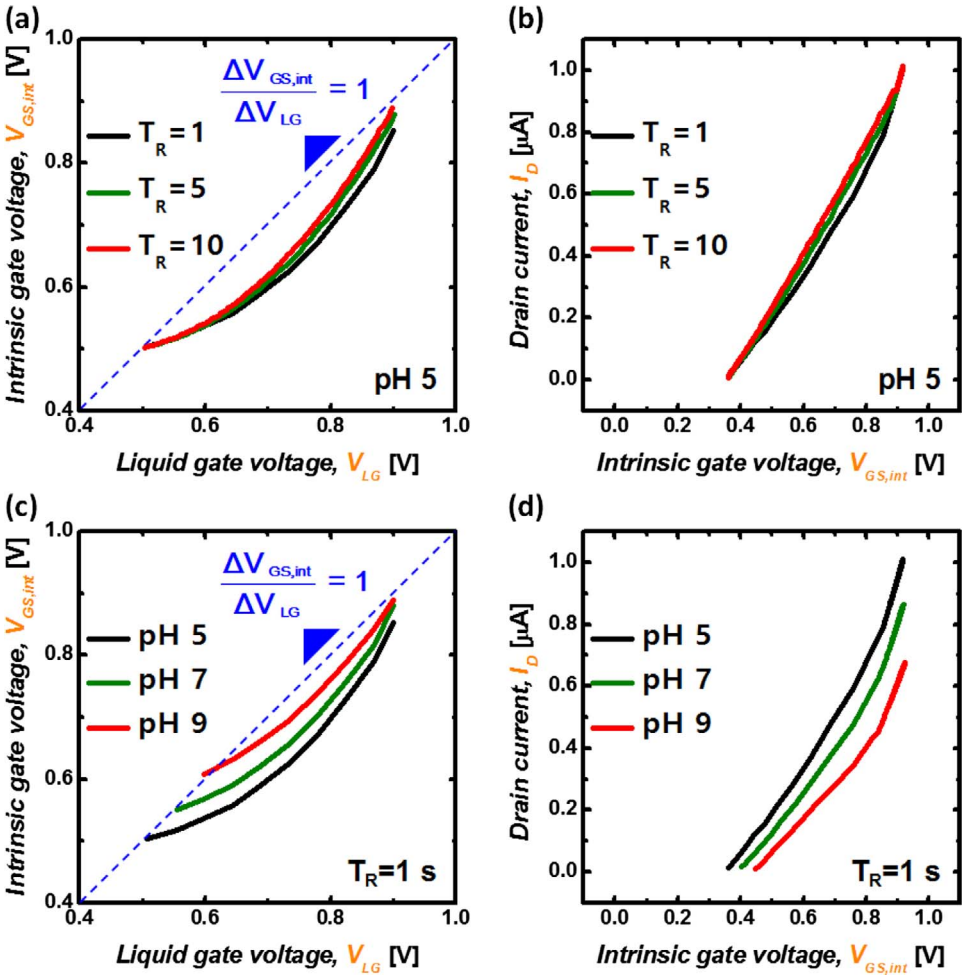

Fig. 4. (a) V_{LG}-$V_{GS,int}$ under the different T_R at a constant pH 5. (b) $V_{GS,int}$-I_D under the different T_R at a constant pH 5. (c) V_{LG}-$V_{GS,int}$ under the different pH at a constant T_R. (d) $V_{GS,int}$-I_D under the different pH at a constant T_R.

our previous works [8,13,15], herein the transient response of ISFETs is paid attention to rather than the sensitivity itself in DC response. More importantly, it should be noted that our main conclusions, including explanation, model, and method, will be generally available irrespective of the ISFET sensitivity.

The pH-sensing signal needs to be acquired after waiting for at least a certain amount of time, called the saturation time, if it takes a significant time for the I_D to reach a steady-state value after the time-varying V_{LG} is setup. To systematically determine the optimal saturation time, the transient I_D was measured at a fixed V_D = 0.9 V, while V_{LG} was ramped up from 0 V to 0.9 V during T_R, as illustrated in Fig. 3(a). Here T_R was varied over 0.2, 1, 5, and 10 s. In this way, the transient I_D was measured with varying T_R and pH, as seen in Fig. 3(b). The saturation time (t_{sat}) was defined as the time difference between the time spot when V_{LG} arrived at 0.9 V and $t_{sat,end}$. The saturation time was symbolized as t_{sat} and the time spot at $\partial I_D/\partial t$ = 1 nA/s ($t_{sat,end}$) which means the moment when I_D reached at the pH-dependent steady-state value, as indicated in Fig. 3(b). The measured I_Ds as the function of pH and T_R are summarized in Fig. 3(d), and the experimentally extracted t_{sat} is shown in Fig. 3(c) and Table 1.

V_T is dependent on the pH value and is within the range of 0.5–0.6 V (Fig. 3(d)). Our measurement satisfies the condition of $V_{GS,int}(t) \leq V_{LG}(t)$, and the maximum value of V_{LG} is a constant V_D value of 0.9 V. Therefore, our ISFET operates in a saturation region only if $V_{GS,int} > V_T$, so $I_D \propto (V_{GS,int} - V_T)^2$. The $V_{GS,int}$ value during T_R can be then extracted using $I_D(t)$ / I_D ($t = t_{sat,end}$) = $(V_{GS,int} - V_T)^2/(0.9 - V_T)^2$ because the $V_{GS,int}$ value is 0.9 V, i.e., the maximum V_{LG} value at $t = t_{sat,end}$. $V_{GS,int}(t)$ is synchronously correlated with $V_{LG}(t)$ at a constant pH of 5 as a function of T_R (Fig. 4(a)) and is also correlated with $V_{LG}(t)$ at a constant T_R = 1 s as a function of pH (Fig. 4(c)), respectively. As seen in Fig. 4(a) and (c), $I_D(t)$ versus $V_{GS,int}(t)$ during T_R is also shown in Fig. 4(b) and (d).

3. Results and discussion

The rate of time-varying I_D can be formulated as follows:

$$\frac{\partial I_D(t)}{\partial t} = \frac{\partial V_{LG}(t)}{\partial t} \times \frac{\partial V_{GS,int}(t)}{\partial V_{LG}(t)} \times \frac{\partial I_D(t)}{\partial V_{GS,int}(t)} \quad (1)$$

where the first term of the right-hand side increases as T_R becomes shorter. The second term suggests the delay of $V_{GS,int}$ in response to the time-varying V_{LG}, which is due to the retardation of mobile ions in the electrolyte.

In the transient model of ISFETs, the second term is frequently modeled by combining the electrolyte resistance, double-layer capacitance, stern capacitance, and the capacitance due to the charging/discharging of the surface ionizable groups [19]. However, the second term should be carefully modeled because the electrolyte and the FET cannot be decoupled from each other, and the relation between $V_{GS,int}$ and V_{LG} is complicatedly non-linear.

Furthermore, our observation in Fig. 4 suggests that the second term depends on either the first term ($\partial V_{LG}/\partial t$) or the pH. In the case of short T_R, mobile ions cannot respond to the time-varying speed of V_{LG}. It is also noteworthy that as mobile ions drift more quickly to the electrolyte/gate oxide interface, in other words, the more abruptly proton ion concentration, i.e., $[H^+]$, increases at the electrolyte/gate oxide interface, the larger the flux of ions diffuses backward away from the electrolyte/gate oxide interface. It takes a longer time, therefore, for I_D to

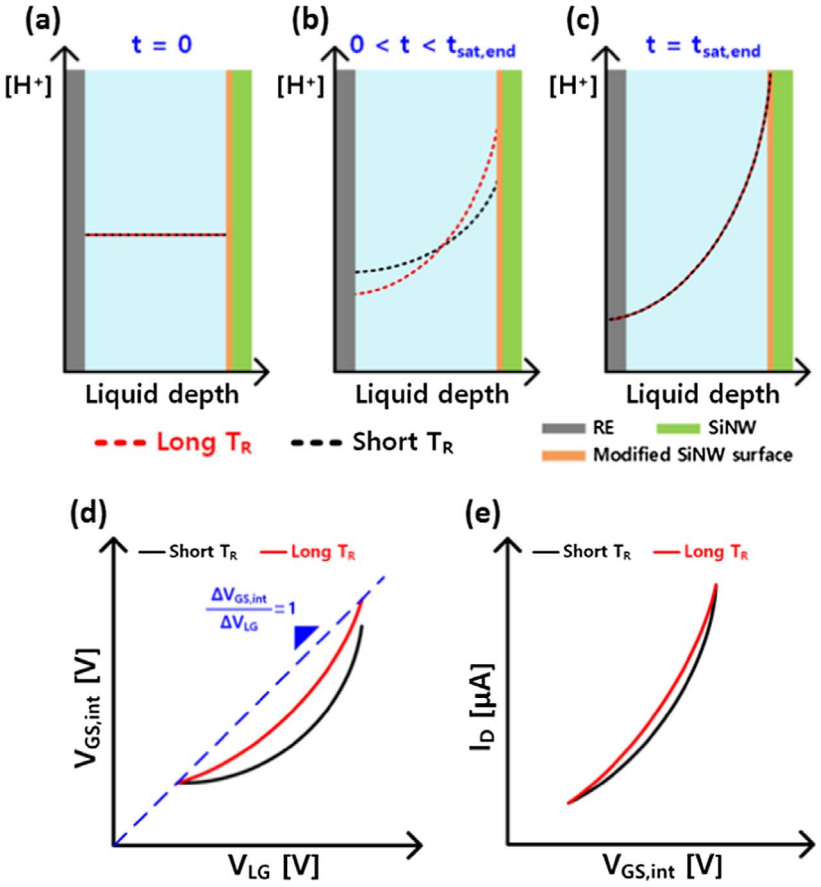

Fig. 5. Proton ion concentration ([H^+]) in the electrolyte/gate oxide interface from different T_R at (a) t = 0, (b) 0 < t < $t_{sat,end}$, and (c) t = $t_{sat,end}$. Illustration of relation (d) between V_{LG} and $V_{GS,int}$ and (e) between $V_{GS,int}$ and I_D from different T_R.

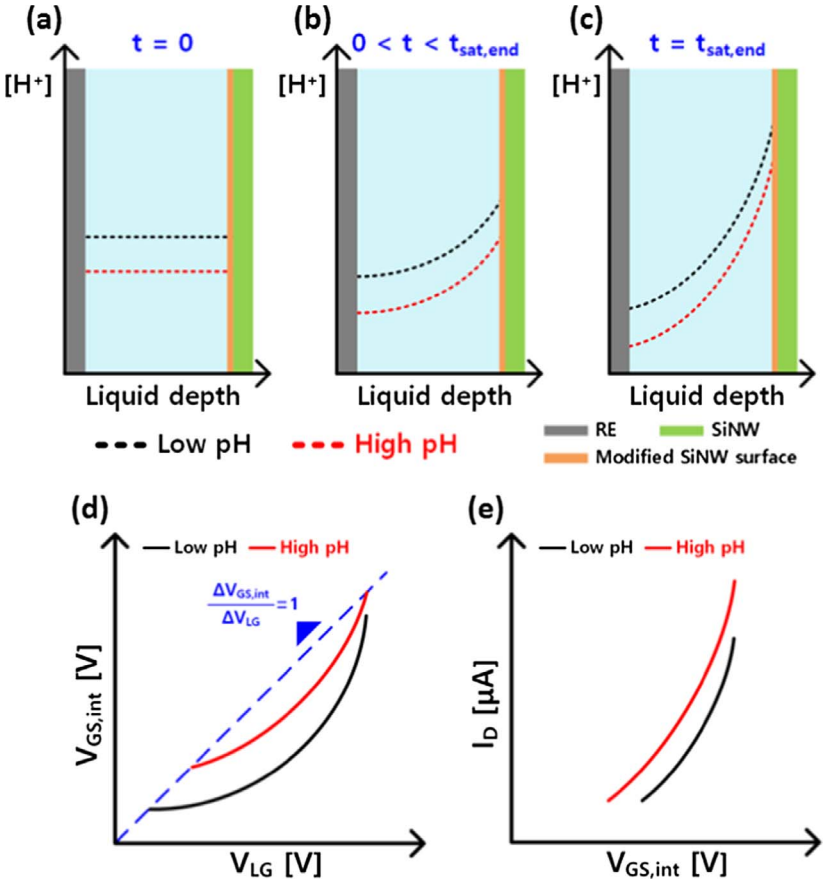

Fig. 6. Proton ion concentration ([H^+]) in the electrolyte/gate oxide interface from different pH at (a) t = 0, (b) 0 < t < $t_{sat,end}$, and (c) t = $t_{sat,end}$. Illustration of relation (d) between V_{LG} and $V_{GS,int}$ and (e) between $V_{GS,int}$ and I_D from different pH.

reach the steady-state value, i.e., t_{sat} increases, because the I_D reaches a steady-state after the drift and diffusion of mobile ions balance each other, as shown in Fig. 5(a)–(c). Consequently, during T_R, the $V_{GS,int}$ is more deviated from the V_{LG} in a short T_R case rather than in a long T_R case, as observed in Fig. 4(a) and as illustrated in Fig. 5(d) and (e). With respect to T_R dependence, our model is highly consistent with the observations in Fig. 3 and Table 1.

The rate of $\partial V_{GS,int}/\partial V_{LG}$ also depends on the $[H^+]$ concentration of electrolyte, i.e., the pH value. As the $[H^+]$ increases and the pH gets lower, it takes a longer time for the drift and diffusion of mobile ions to be balanced by each other and the t_{sat} increases, as illustrated in Fig. 6(a)–(c). Consequently, during T_R, $V_{GS,int}$ deviates more from V_{LG} in a low pH case rather than in a high pH case as observed in Figs. 4(c), 6(d), and (e). Our model is also consistent with the observation in Fig. 3 and Table 1 in terms of pH dependence.

Therefore, a longer hold time for V_{LG} biasing is required as the T_R becomes shorter and the pH decreases.

4. Conclusion

The influence of both T_R of V_{LG} and pH on the transient I_D response has been experimentally investigated in SiNW ISFET-based pH sensors. As T_R becomes shorter and the pH value decreases, it takes a longer time for the ISFET current to saturate to the pH-dependent steady-state value. Before the time arrives at $t = t_{sat,end}$, $V_{GS,int}$ deviates more from V_{LG} in either of the two cases, the shorter T_R case or the lower pH case. Our model, which is based on the time taken for mobile ions in the electrolyte to be balanced between drift and diffusion, explains the observation very well. Our results supply the experimental background for more exact transient ISFET modeling, e.g., double-layer, stern, and charging/discharging capacitance, and give useful insights on the design of rising time of V_{LG} bias in ISFET-based point-of-care circuits and systems.

Acknowledgement

This work was supported by the National Research Foundation of Korea (NRF) grant funded by the Korea government (Ministry of Education, Science and Technology, MEST) (Nos. 2016R1A5A1012966 and 2016R1A6A3A01006588). The CAD software was supported by SYNOPSYS and IDEC.

Reference

[1] Singer, Richard B, Hastings AB. An improved clinical method for the estimation of disturbances of the acid-base balance of human blood. Medicine 1948;27:223.
[2] Majumdar S, Srirangam R. Solubility, Stability, Physicochemical Characteristics and In Vitro Ocular Tissue Permeability of Hesperidin: A Natural Bioflavonoid. Pharmaceut Res 2009;26:1217–25. http://dx.doi.org/10.1007/s11095-008-9729-6.
[3] Harter Robert D. Effect of soil pH on adsorption of lead, copper, zinc, and nickel. Soil Sci Soc Am J 1983;47:47–51. http://dx.doi.org/10.2136/sssaj1983.03615995004700010009x.
[4] Bergveld P. Thirty years of ISFETOLOGY What happened in the past 30 years and what may happen in the next 30 years. Sensors Actuat B: Chem 2003;88:1–20. http://dx.doi.org/10.1016/S0925-4005(02)00301-5.
[5] Rothberg JM, Hinz W, Rearick TM, Schultz J, Mileski W, Davey M, et al. An integrated semiconductor device enabling non-optical genome sequencing. Nature 2011;475:348–52. http://dx.doi.org/10.1038/nature10242.
[6] Toumazou C, Shepherd LM, Reed SC, Chen GI, Patel A, Garner DM, et al. Simultaneous DNA amplification and detection using a pH-sensing semiconductor system. Nat Methods 2013;10:641–6. http://dx.doi.org/10.1038/nmeth.2520.
[7] Lallement G, Moser N, Georgiou P. Bio-inspired pH sensing using Ion Sensitive Field Effect Transistors. Circuits and Systems (ISCAS) 2016:2835–38. doi:10.1109/ISCAS.2016.7539183.
[8] Lee J, Lee JM, Lee JH, Lee WH, Uhm M, Park BK, et al. Complementary silicon nanowire hydrogen ion sensor with high sensitivity and voltage output. IEEE Electron Device Lett 2012;33:1768–70. http://dx.doi.org/10.1109/LED.2012.2220515.
[9] Yen LC, Pan TM, Lee CH, Chao TS. Label-free and real-time detection of ferritin using a horn-likepolycrystalline-silicon nanowire field-effect transistor biosensor. Sens Actuat B: Chem 2016;203:398–404. http://dx.doi.org/10.1016/j.snb.2016.02.095.
[10] Gao XP, Zheng G, Lieber CM. Subthreshold Regime has the Optimal Sensitivity for Nanowire FET Biosensors. Nano Lett 2009;10:547–52. http://dx.doi.org/10.1021/nl9034219.
[11] Cui Y, Wei Q, Park H, Lieber CM. Nanowire nanosensors for highly sensitive and selective detection of biological and chemical species. Science 2001;293:1289–92. http://dx.doi.org/10.1126/science.1062711.
[12] Stern E, Klemic JF, Routenberg DA, Wyrembak PN, Turner-Evans DB, Hamilton AD, et al. Label-free immunodetection with CMOS-compatible semiconducting nanowires. Nature 2007;445:519–22. http://dx.doi.org/10.1038/nature05498.
[13] Lee J, Jang J, Choi B, Yoon J, Kim JY, Choi YK, et al. A highly responsive silicon nanowire/amplifier MOSFET Hybrid biosensor. Sci Rep 2015;5:12286. http://dx.doi.org/10.1038/srep12286.
[14] Lee J, Lee JM, Lee JH, Uhm M, Lee WH, Hwang S, et al. SiNW-CMOS hybrid common-source amplifier as a voltage-readout hydrogen ion sensor. IEEE Electron Device Lett 2013;34:135–7. http://dx.doi.org/10.1109/LED.2012.2226136.
[15] Lee J, Hwang S, Choi B, Lee JH, Moon DI, Seol ML, et al. A Novel SiNW/CMOS Hybrid Biosensor for High Sensitivity/Low Noise. In Electron Devices Meeting (IEDM) 2013:14–5. doi:10.1109/IEDM.2013.6724631.
[16] Choi B, Lee J, Yoon J, Ahn JH, Park TJ, Kim DM, et al. TCAD-based simulation method for the electrolyte–insulator–semiconductor field-effect transistor. IEEE Trans Electron Dev 2015;62:1072–5. http://dx.doi.org/10.1109/TED.2015.2395875.
[17] Cui D, Qian X, Liu F, Zhang R. Novel fluorescent ph sensors based on intramolecular hydrogen bonding ability of Naphthalimide. Org Lett 2004;6:2757–60. http://dx.doi.org/10.1021/ol049005h.
[18] Bousse L, De Rooij NF, Bergveld P. Operation of chemically sensitive field-effect sensors as a function of the insulator-electrolyte interface. IEEE Trans Electron Devices 1983;30:1263–70. http://dx.doi.org/10.1109/T-ED.1983.21284.
[19] Lee WH, Lee JM, Uhm M, Lee J, Kim KR, Choi SJ, et al. Characterization and capacitive modeling of target concentration-dependent subthreshold swing in silicon Nanoribbon biosensors. IEEE Electron Device Lett 2014;35:587–9. http://dx.doi.org/10.1109/LED.2014.2312196.